ANNUAL REVIEWS

Annual Review of Condensed Matter Physics

Higgs Mode in Superconductors

Ryo Shimano[1,2] and Naoto Tsuji[3]

[1]Cryogenic Research Center, The University of Tokyo, Tokyo 113-0032, Japan; email: shimano@phys.s.u-tokyo.ac.jp

[2]Department of Physics, The University of Tokyo, Tokyo 113-0033, Japan

[3]RIKEN Center for Emergent Matter Science (CEMS), Wako 351-0198, Japan; email: naoto.tsuji@riken.jp

Annu. Rev. Condens. Matter Phys. 2020. 11:103–24

First published as a Review in Advance on September 30, 2019

The *Annual Review of Condensed Matter Physics* is online at conmatphys.annualreviews.org

https://doi.org/10.1146/annurev-conmatphys-031119-050813

Keywords

superconductivity, collective modes, terahertz spectroscopy, ultrafast phenomena, nonequilibrium dynamics, spontaneous symmetry breaking

Abstract

When the continuous symmetry of a physical system is spontaneously broken, two types of collective modes typically emerge: the amplitude and the phase modes of the order-parameter fluctuation. For superconductors, the amplitude mode is referred to most recently as the Higgs mode as it is a condensed-matter analog of a Higgs boson in particle physics. Higgs mode is a scalar excitation of the order parameter, distinct from charge or spin fluctuations, and thus does not couple to electromagnetic fields linearly. This is why the Higgs mode in superconductors has evaded experimental observations for over a half century after the initial theoretical prediction, except for a charge-density-wave coexisting system. With the advance of nonlinear and time-resolved terahertz spectroscopy techniques, however, it has become possible to study the Higgs mode through the nonlinear light–Higgs coupling. In this review, we overview recent progress in the study of the Higgs mode in superconductors.

1. INTRODUCTION AND A BRIEF HISTORICAL OVERVIEW

Spontaneous breaking of a continuous symmetry is a fundamental concept of phase transition phenomena in various physical systems ranging from condensed matter to high-energy physics (1). For instance, a ferromagnetic transition is characterized by the spontaneous breaking of spin rotational symmetry. Likewise, superconductivity is characterized by the spontaneous breaking of U(1) rotational symmetry with respect to the phase of a macroscopic wavefunction (2).

When a continuous symmetry is spontaneously broken, there emerge two types of collective modes in general: fluctuations of the phase and amplitude of the order parameter as schematically shown in **Figure 1*a***. The phase mode also termed Nambu–Goldstone or NG mode is primarily a gapless (massless) mode (3–8) as required by the symmetry. An acoustic phonon is an example that is associated with spontaneous breaking of translational symmetry in a crystal lattice. The amplitude mode, however, is generally a gapped (massive) mode because its excitation costs a finite energy due to the presence of the potential curvature along the radial direction (**Figure 1*a***). The amplitude mode (especially for superconductors) is often called the Higgs mode according to the close analogy with the Higgs boson in particle physics. It may sound strange that one talks about the Higgs particle in condensed matter systems, but in fact the origin of the idea of Higgs physics can be found in the course of the study of superconductivity (3–9). Namely, the standard model in particle physics can be viewed as a relativistic version of the Ginzburg–Landau (GL) theory (2), i.e., a low-energy effective theory of superconductors. The emergence of the Higgs mode is a universal and fundamental phenomenon in systems with spontaneous symmetry breaking.

The Higgs mode occupies a special status for superconductors in which the order parameter couples to gauge fields because it is the lowest-energy collective excitation mode (**Figure 1*b***). The massless phase mode is absorbed into the longitudinal component of electromagnetic fields and is lifted to high energy in the scale of the plasma frequency due to the Anderson–Higgs mechanism (4–6, 9–13). As a result, the amplitude mode becomes stable against the decay to the phase mode in superconductors. The existence of the amplitude mode in superconductors was suggested by Anderson (5, 14) soon after the development of a microscopic theory of superconductivity by

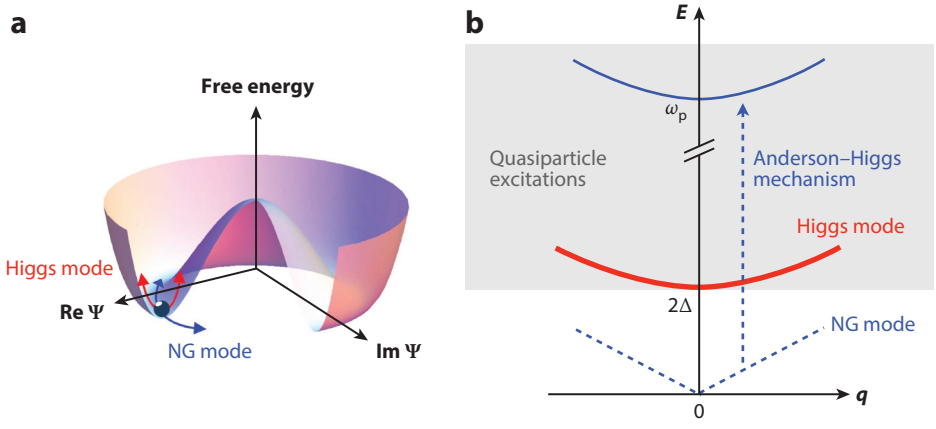

Figure 1

(*a*) A schematic picture of the Higgs (*red*) and NG (*blue*) modes represented on the Mexican-hat free-energy potential as a function of the complex order parameter Ψ. (*b*) A schematic excitation spectrum of an *s*-wave superconductor. Due to the Anderson–Higgs mechanism, the NG mode acquires an energy gap in the order of the plasma frequency ω_p, whereas the Higgs mode remains in low energy with an energy gap 2Δ, above which the quasiparticle excitation continuum overlaps. Abbreviation: NG, Nambu–Goldstone.

Bardeen, Cooper, and Schrieffer (BCS) (15). In an *s*-wave (BCS-type) superconductor, the Higgs-mode energy ω_{H} coincides with the superconducting gap energy 2Δ (5, 15a–19; see also 20, 21). This is eventually consistent with Nambu's conjectural sum rule (21, 22): $\omega_{\mathrm{H}}^2 + \omega_{\mathrm{NG}}^2 = 4\Delta^2$ with the NG mode energy $\omega_{\mathrm{NG}} = 0$. Because the Higgs mode lies at the lower bound of the quasiparticle continuum near zero momentum, the decay of the Higgs mode to single-particle excitations is suppressed and becomes a much slower power law (16). For nonzero momentum, the Higgs mode can decay by transferring its energy to quasiparticle excitations. The energy dispersion and the damping rate of the Higgs mode has been derived within the random phase approximation (18, 19).

Given that the theory of the Higgs particle originates from that of superconductivity and that the Higgs particle was discovered in large hadron collider (LHC) experiments in 2012 (23, 24), it is rather surprising that an experimental observation of the Higgs mode in superconductors, a home ground of Higgs physics, has been elusive for a long time. There are, however, good reasons for this: The Higgs mode does not have any electric charge, electric dipole, magnetic moment, and other quantum numbers. In other words, the Higgs mode is a scalar excitation (which is distinct from, e.g., charge fluctuations). Therefore, it does not couple to external probes such as electromagnetic fields in the linear-response regime. Another reason is that the energy scale of the Higgs mode lies in that of the superconducting gap, which is in the order of millielectron volts in typical metallic superconductors. To excite the Higgs mode, one needs an intense terahertz (THz) light source (1 THz $\sim$ 4 meV $\sim$ 300 μm), which has become available only in the past decade.

One exception (and the first case) for the observation of the Higgs mode in superconductors in the early stages was the Raman scattering experiment for a superconductor 2H-$NbSe_2$ (25, 26). It is exceptional in the sense that superconductivity and charge-density wave (CDW) coexist in a single material. The Raman peak observed near the superconducting gap energy 2Δ in 2H-$NbSe_2$ was first interpreted as a single-particle excitation across the gap (25, 26). Later, Littlewood & Varma (18, 19) theoretically elucidated that the peak corresponds to the scalar excitation of the amplitude mode (i.e., the Higgs mode; see also Reference 27). A renewed interest in the Raman signal has recently revealed the importance of the coexisting CDW order for the Higgs mode to be visible in the Raman response (28–30). Indeed, the Raman peak of the Higgs mode has been shown to be absent in a superconducting NbS_2, which is a material similar to $NbSe_2$ but has no CDW order (28).

A long-standing issue is whether the Higgs mode can be observed in superconductors without CDW order. On the theoretical side, there have been various proposals for the excitation of the Higgs mode, including quench dynamics (16, 31–37) as well as laser excitation (38–44). It is only after the development of ultrafast pump-probe spectroscopy techniques in the low-energy THz-frequency region that a clear observation of the Higgs-mode oscillation has been reported in a pure *s*-wave superconductor NbN (45) (with "pure" meaning no other long-range order such as CDW). Subsequently, the Higgs mode was experimentally demonstrated to couple to electromagnetic fields in a nonlinear way through the THz pump-probe and third harmonic generation (THG) measurements (46). In the THG experiment, a resonant enhancement of THG was discovered (46) at the condition $2\omega = 2\Delta$ with ω being the frequency of the incident THz light, indicating the nonlinear light–Higgs coupling in a two-photon process (42).

Meanwhile, it has been theoretically pointed out that not only the Higgs mode but also charge-density fluctuation (CDF) can contribute to the THG signal (47). The CDF generally gives a much larger contribution than the Higgs mode in a clean-limit superconductor within the BCS mean-field approximation. Whereas the relative magnitude of the Higgs-mode and CDF contributions to the THG has been under debate (47–50), theoretical progress has recently been made on the theory of the light–Higgs coupling, showing that the effects of both phonon

retardation (48) and nonmagnetic impurity scattering (51–54) drastically enhance the Higgs-mode contribution to nonlinear optical responses, which far exceeds the CDF contribution.

The experiments have been extended to high-T_c cuprate superconductors, showing the presence of the Higgs-mode contribution to the pump-probe signal in d-wave superconductors (55). Recently the THG has also been identified in various high-T_c cuprates (56). The Higgs mode can be made visible in a linear optical response if dc supercurrent is flowing in a superconductor (57). The IR-activated Higgs mode in the presence of supercurrents has recently been observed in a superconductor NbN (58).

In this review article, we overview recent progress in the study of the Higgs mode in superconductors (where the Anderson–Higgs mechanism is taking place), with an emphasis on the experimental aspects. In a broader context, collective amplitude modes are not limited to superconductors but are ubiquitous in condensed matter systems that may not be coupled to gauge fields (hence without the Anderson–Higgs mechanism). Those include squashing modes in superfluid ^{3}He (59), amplitude modes in bosonic and fermionic condensates of ultracold-atom systems (60, 61), amplitude modes in quantum antiferromagnets (62), and so on. A comprehensive review including these topics can be found in Reference 63.

2. NONLINEAR LIGHT–HIGGS COUPLING

In this section, we review from a theoretical point of view how the Higgs mode in superconductors couples to electromagnetic fields in a nonlinear way. It is important to understand the mechanism of the nonlinear light–Higgs coupling for observing the Higgs mode in experiments. In fact, the Higgs mode does not have a linear response against electromagnetic fields in usual situations, which has been a longtime obstacle for detecting the Higgs mode in superconductors.

2.1. A Phenomenological View

Let us first take a phenomenological point of view based on the GL theory (2), which provides us with a quick look at the nonlinear light–Higgs coupling. For early developments based on the time-dependent GL theory, we refer to References 64–68. In the GL theory, the free-energy density f is assumed to be a functional of a complex order-parameter field $\psi(\mathbf{r})$,

$$f[\psi] = f_0 + a|\psi(\mathbf{r})|^2 + \frac{b}{2}|\psi(\mathbf{r})|^4 + \frac{1}{2m^*}|(-i\nabla - e^*\mathbf{A})\psi(\mathbf{r})|^2, \qquad 1.$$

where $a = a_0(T - T_c)$, a_0 and b are some constants, m^* and e^* are the effective mass and the effective charge of the Cooper pair condensate, and $\mathbf{A}$ is the vector potential that represents the external light field [$\mathbf{E}(t) = -\partial\mathbf{A}(t)/\partial t$]. The amplitude of the order parameter corresponds to the superfluid density (i.e., $|\psi|^2 = n_s$), whereas the phase corresponds to that of the condensate.

The free-energy density (Equation 1) is invariant under the global U(1) phase rotation $\psi(\mathbf{r}) \to e^{i\varphi}\psi(\mathbf{r})$ and more generally under the gauge transformation $\psi(\mathbf{r}) \to e^{ie^*\chi(\mathbf{r})}\psi(\mathbf{r})$, with $\mathbf{A}(\mathbf{r}) \to \mathbf{A}(\mathbf{r}) + \nabla\chi(\mathbf{r})$ for an arbitrary scalar field $\chi(\mathbf{r})$. In addition, the GL free-energy density (Equation 1) is invariant against the particle–hole transformation $\psi(\mathbf{r}) \to \psi^\dagger(\mathbf{r})$. The presence of the particle–hole symmetry (including the time derivative terms in the action) is crucial (27, 63, 69) in decoupling the Higgs amplitude mode from the phase mode (NG mode) in electrically neutral systems such as superfluid ultracold atoms. Without the particle–hole symmetry, the Higgs mode quickly decays into the phase mode and becomes short-lived. In superconductors (which consist of electrically charged electrons), by contrast, the phase mode acquires an energy gap on the order of the plasma frequency due to the Anderson–Higgs mechanism. This prevents the Higgs

mode from decaying into the phase mode. The particle–hole symmetry itself is realized as an approximate symmetry in the Bogoliubov–de Gennes Hamiltonian, which describes microscopic low-energy physics of superconductors around the Fermi energy at the mean-field level.

When the temperature goes below the critical temperature (i.e., $a < 0$), the global U(1) symmetry is spontaneously broken, and the system turns into a superconducting state. The order-parameter fluctuation from the ground state [$\psi(\mathbf{r}) = \psi_0$] can be decomposed into amplitude $H(\mathbf{r})$ and phase $\theta(\mathbf{r})$ components,

$$\psi(\mathbf{r}) = [\psi_0 + H(\mathbf{r})]e^{i\theta(\mathbf{r})}. \quad 2.$$

Then, the GL potential can be expressed up to the second order of the fluctuation as

$$f = -2aH^2 + \frac{1}{2m^*}(\nabla H)^2 + \frac{e^{*2}}{2m^*}\left(\mathbf{A} - \frac{1}{e^*}\nabla\theta\right)^2 (\psi_0 + H)^2 + \ldots. \quad 3.$$

The first term on the right-hand side of Equation 3 indicates that the Higgs mode has an energy gap (**Figure 1*b***) proportional to $(-a)^{1/2} \propto (T_c - T)^{1/2}$. The microscopic BCS mean-field theory predicts that the Higgs gap is identical to the superconducting gap 2Δ (5, 15a–19). The phase field $\theta(\mathbf{r})$ does not have such a mass term, so at first sight one would expect to have a massless NG mode. However, $\theta(\mathbf{r})$ always appears in the form of $(\mathbf{A} - \nabla\theta/e^*)$ in Equation 3, which allows one to eliminate $\theta(\mathbf{r})$ from the GL potential by taking a unitary gauge $\mathbf{A}' = \mathbf{A} - \nabla\theta/e^*$. As a result, we obtain (denoting $\mathbf{A}'$ as $\mathbf{A}$)

$$f = -2aH^2 + \frac{1}{2m^*}(\nabla H)^2 + \frac{e^{*2}\psi_0^2}{2m^*}\mathbf{A}^2 + \frac{e^{*2}\psi_0}{m^*}\mathbf{A}^2 H + \ldots. \quad 4.$$

One can see that the phase mode is absorbed into the longitudinal component of the electromagnetic field. At the same time, there appears a mass term for photons (the third term on the right-hand side of Equation 4) with the mass proportional to $\sqrt{e^{*2}\psi_0^2/m^*}$ (Anderson–Higgs mechanism). Due to this, electromagnetic waves cannot propagate freely inside superconductors but decay exponentially with a finite penetration length (Meissner effect).

From Equation 4, one immediately sees that there is no linear coupling between the Higgs and electromagnetic field. This is consistent with the fact that the Higgs mode does not have an electric charge, magnetic moment, and other quantum numbers, which has been a main obstacle in observing the Higgs mode by an external probe for a long time. In contrast, there is a nonlinear coupling term $\mathbf{A}^2 H$ in Equation 4 that causes the Higgs mode to contribute in various nonlinear processes. In **Figure 2*a***, we illustrate the diagrammatic representation of the nonlinear light–Higgs coupling, where two photons are coming in with frequencies ω_1 and ω_2 and one Higgs is emitted with frequency $\omega_1 + \omega_2$. This is analogous to the elementary process of the Higgs particle decaying into W bosons that played a role in the discovery of the Higgs particle in LHC experiments (23, 24).

Due to the nonlinear interaction between the Higgs mode and electromagnetic fields, one can induce a nonlinear current given by

$$\mathbf{j} = -\frac{\partial F}{\partial \mathbf{A}} = -\frac{ie^*}{2m^*}[\psi^\dagger\nabla\psi - (\nabla\psi^\dagger)\psi] - \frac{e^{*2}}{m^*}\mathbf{A}\psi^\dagger\psi. \quad 5.$$

Again, we expand ψ around the ground state ψ_0 in Equation 5 and collect leading terms in H, which results in

$$\mathbf{j} = -\frac{2e^{*2}\psi_0}{m^*}\mathbf{A}H. \quad 6.$$

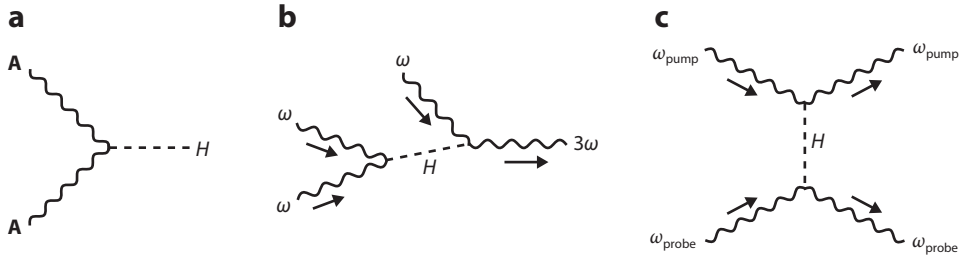

Figure 2

(*a*) Diagrammatic representation of the nonlinear light–Higgs coupling $\mathbf{A}^2 H$ in Equation 4. (*b*) Third harmonic generation mediated by the Higgs mode. (*c*) Pump-probe spectroscopy mediated by the Higgs mode.

This is simply the leading part of the London equation $\mathbf{j} = -(e^{*2} n_s/m^*)\mathbf{A}$ (let us recall that the amplitude of the order parameter corresponds to the superfluid density, $|\psi|^2 = n_s$).

When a monochromatic laser with frequency ω drives a superconductor, the amplitude of the order parameter oscillates with frequency 2ω due to the nonlinear coupling $\mathbf{A}^2 H$ (**Figure 2*a***). Together with the oscillation of $\mathbf{A}$ with frequency ω in Equation 6, the induced nonlinear current shows an oscillation with frequency 3ω. As a result, one obtains the THG mediated by the Higgs mode (**Figure 2*b***). Because the Higgs mode has an energy 2Δ at low momentum, one can resonantly excite the Higgs mode by a THz laser with a resonance condition $2\omega = 2\Delta$. Given that the nonlinear current is proportional to the Higgs-mode amplitude (Equation 6), the third harmonic generation can be resonantly enhanced through the excitation of the Higgs mode. The Higgs-mode resonance in THG has been experimentally observed for a conventional superconductor (46).

Another example of nonlinear processes to which the Higgs mode can contribute is pump-probe spectroscopy in which pump and probe light are simultaneously applied (**Figure 2*c***). In this case, photons with different frequencies $\omega_{\rm pump}$ and $\omega_{\rm probe}$ are injected, and those with the same respective frequencies are emitted. There are three possibilities of the frequency carried by the Higgs mode: $\omega_{\rm pump} \pm \omega_{\rm probe}$ and $\omega_{\rm pump} - \omega_{\rm pump} = \omega_{\rm probe} - \omega_{\rm probe} = 0$. If one uses a THz pump and optical probe, i.e., $\omega_{\rm pump} \lesssim 2\Delta$ and $\omega_{\rm probe} \gg 2\Delta$, the first two channels do not contribute because the excitation of the Higgs mode is far off-resonant. The remaining zero-frequency excitation channel contributes to the pump-probe spectroscopy. This process has been elaborated in the experimental study of the Higgs mode in *d*-wave superconductors (55).

2.2. A Microscopic View

In the previous subsection, we reviewed the phenomenology for the nonlinear light–Higgs coupling using the GL theory. However, strictly speaking, the application of the GL theory to nonequilibrium problems is not microscopically justified in the case of gapped superconductors (70–72). The reason is that in a usual situation one cannot neglect the effect of quasiparticle excitations whose relaxation time is longer than the timescale of the order-parameter variation. Furthermore, the Higgs mode and quasiparticle excitations are energetically degenerate at low momentum (**Figure 1*b***), so it is inevitable to excite quasiparticles at the same time when one excites the Higgs mode. This motivates us to take a microscopic approach for further understanding.

Let us adopt the time-dependent BCS or Bogoliubov–de Gennes equation, which is efficiently represented by the Anderson pseudospin $\boldsymbol{\sigma}_{\mathbf{k}} = \frac{1}{2}\langle \Psi_{\mathbf{k}}^\dagger \boldsymbol{\tau} \Psi_{\mathbf{k}} \rangle$ (5). Here, $\Psi_{\mathbf{k}}^\dagger = (c_{\mathbf{k}\uparrow}^\dagger, c_{-\mathbf{k}\downarrow})$ is the Nambu spinor, $\boldsymbol{\tau} = (\tau_x, \tau_y, \tau_z)$ are Pauli matrices, $c_{\mathbf{k}\sigma}^\dagger$ ($c_{\mathbf{k}\sigma}$) is the creation (annihilation) operator of

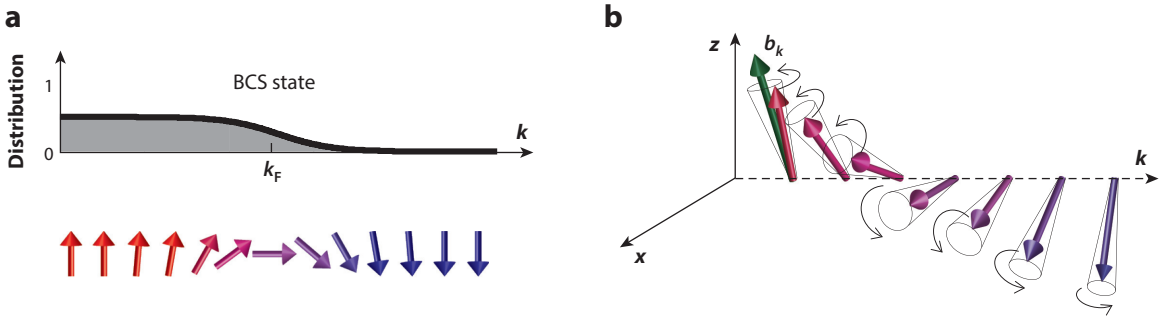

Figure 3

(*a*) Momentum distribution of a superconducting state (*upper*) and its pseudospin representation due to Anderson (*lower*). (*b*) Pseudospin precession induced by a laser field. Panels adapted from Reference 46 with permission. Abbreviation: BCS, Bardeen–Cooper–Schrieffer.

electrons with momentum $\mathbf{k}$ and spin σ, and $\langle \cdots \rangle$ denotes the statistical average. Physically, the x and y components of the Anderson pseudospin correspond to the real and imaginary parts of the Cooper pair density, respectively, and the z component corresponds to the momentum occupation distribution of electrons (**Figure 3*a***). With this notation, the BCS mean-field Hamiltonian is written as

$$H_{\mathrm{BCS}} = 2\sum_{\mathbf{k}} \mathbf{b}_{\mathbf{k}}(t)\cdot\boldsymbol{\sigma}_{\mathbf{k}}, \qquad 7.$$

$$\mathbf{b}_{\mathbf{k}}(t) = \left\{ -\Delta'(t), -\Delta''(t), \frac{1}{2}[\epsilon_{\mathbf{k}+\mathbf{A}(t)} + \epsilon_{\mathbf{k}-\mathbf{A}(t)}] \right\}. \qquad 8.$$

Here, $\mathbf{b}_{\mathbf{k}}(t)$ is a pseudomagnetic field acting on pseudospins; Δ' and Δ'' are the real and imaginary parts of the superconducting gap function, respectively; and $\epsilon_{\mathbf{k}}$ is the band dispersion of the system. The equation of motion for the pseudospins is given by the Bloch-type equation,

$$\frac{\partial}{\partial t}\boldsymbol{\sigma}_{\mathbf{k}}(t) = 2\mathbf{b}_{\mathbf{k}}(t)\times\boldsymbol{\sigma}_{\mathbf{k}}(t), \qquad 9.$$

supplemented by the mean-field condition $\Delta'(t) + i\Delta''(t) = \frac{V}{N}\sum_{\mathbf{k}}[\sigma^x_{\mathbf{k}}(t) + i\sigma^y_{\mathbf{k}}(t)]$ with V the attractive interaction and N the number of k points. The time evolution of the superconducting state is thus translated into the precession dynamics of Anderson pseudospins (**Figure 3*b***).

The coupling to the electromagnetic field appears in the z component of the pseudomagnetic field, $b^z_{\mathbf{k}} = \frac{1}{2}[\epsilon_{\mathbf{k}+\mathbf{A}(t)} + \epsilon_{\mathbf{k}-\mathbf{A}(t)}]$. If we expand $b^z_{\mathbf{k}}$ in terms of $\mathbf{A}(t)$, we obtain $b^z_{\mathbf{k}} = \epsilon_{\mathbf{k}} + \frac{1}{2}\sum_{ij}\frac{\partial^2\epsilon_{\mathbf{k}}}{\partial k_i \partial k_j}A_iA_j + O(A^4)$. The linear coupling term vanishes, which is consistent with the phenomenology that we have reviewed in Section 2.1. The leading nonlinear coupling term is quadratic in $\mathbf{A}(t)$. In **Figure 4*a***, we show a numerical result for the time evolution of the gap function $\Delta(t)$ when the system is driven by a multicycle electric-field pulse. One can see that the 2ω oscillation of the gap is generated during the pulse irradiation, after which a free gap oscillation continues with the frequency 2Δ and the amplitude slowly damping as $t^{-1/2}$ (16).

For a monochromatic wave $\mathbf{A}(t) = \mathbf{A}_0 \sin\omega t$, one can solve the equation of motion semianalytically by linearizing with respect to the quadratic coupling $A_i(t)A_j(t)$ around the equilibrium solution. The result shows that the amplitude of the gap function varies as (42)

$$\delta\Delta(t) \propto |2\omega - 2\Delta|^{-\frac{1}{2}}\cos(2\omega t - \phi) \qquad 10.$$

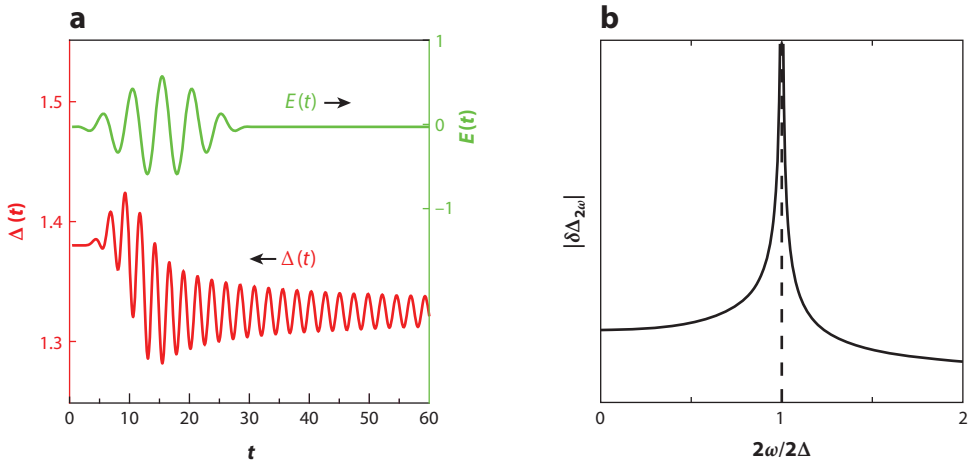

Figure 4

(*a*) A numerical result for the time evolution of the superconducting gap $\Delta(t)$ driven by an electric field pulse $E(t)$ with the frequency $\omega = 2\pi/5 \sim 1.26$. Here, we take a two-dimensional square lattice with a bandwidth 8 at half filling. The interaction is $V = 4$, and the initial temperature is $T = 0.02$. The polarization of the electric field is parallel to the x axis. The left (right) vertical axis represents the value of $\Delta(t)$ [$E(t)$] as indicated by the arrows. (*b*) The amplitude of the 2ω oscillation of the superconducting gap as a function of $2\omega/2\Delta$. Panel *b* adapted from Reference 42 with permission.

for $\omega \sim \Delta$, where ϕ is a phase shift. The induced oscillation frequency is 2ω, reflecting the nonlinear coupling between the Higgs mode and electromagnetic fields, $\mathbf{A}^2 H$. The oscillation amplitude diverges when the condition $2\omega = 2\Delta$ is fulfilled (**Figure 4*b***). This is much the same as the spin resonance phenomenon: The forced collective precession of the pseudospins with frequency 2ω due to the nonlinear coupling resonates with the Higgs mode whose energy coincides with 2Δ. The power of the divergence $\frac{1}{2}$ in Equation 10 is smaller than that of a resonance with an infinitely long-lived mode ($\sim|2\omega - \omega_*|^{-1}$). The reason is that the precession gradually dephases due to the momentum-dependent frequency $\omega_{\mathbf{k}} = 2\sqrt{\epsilon_{\mathbf{k}}^2 + \Delta^2}$ for each pseudospin so that the average of the pseudospins $\delta\Delta(t) = \frac{V}{N}\sum_{\mathbf{k}} \delta\sigma_{\mathbf{k}}^x(t)$ shows a power-law damping of oscillations. The phase shift ϕ exhibits a $\frac{\pi}{2}$ jump as one goes across the resonance by changing the drive frequency ω.

In the case of the square lattice and the polarization of the electric field parallel to the diagonal direction in the xy plane, for example, the current is given by $\mathbf{j}(t) \propto \mathbf{A}(t)\delta\Delta(t)$ (42, 46), which corresponds to the phenomenological relation $\mathbf{j}(t) \propto \mathbf{A}(t)H(t)$ (Equation 6). As expected, the Higgs mode induces a resonant enhancement of the THG. However, it has been pointed out (47) that the current relation is valid only in rather special situations such as the square lattice and the polarization parallel to the diagonal direction. In general, the BCS mean-field treatment (in the clean limit) suggests that the Higgs-mode contribution to the THG is subdominant as compared with that of individual quasiparticle excitations. Because the energy scales of the Higgs mode and the quasiparticle pair excitations are in the same order ($\sim 2\Delta$; see **Figure 1*b***), the competition between the two contributions always matters. This point is further examined in the next subsection.

2.3. Impurity and Phonon Assisting

As we have seen in the previous subsection, the Higgs-mode contribution to the THG is generally subdominant in the BCS clean limit. However, there is a growing understanding from recent

studies (48, 49, 51–54) that if one considers effects beyond the BCS mean-field theory in the clean limit (such as impurity scattering and phonon retardation), the light–Higgs coupling strength drastically changes.

To understand the impact of these effects, let us consider the linear optical response. The current induced by a laser field is decomposed into the paramagnetic and diamagnetic components $\mathbf{j} = \mathbf{j}_{\rm para} + \mathbf{j}_{\rm dia}$ with (73)

$$\mathbf{j}_{\rm para} = \sum_{\mathbf{k}\sigma} \frac{\partial \epsilon_{\mathbf{k}}}{\partial \mathbf{k}} \langle c^{\dagger}_{\mathbf{k}\sigma} c_{\mathbf{k}\sigma} \rangle, \qquad 11.$$

$$\mathbf{j}_{\rm dia} = -\sum_{\mathbf{k}\sigma i} \frac{\partial^2 \epsilon_{\mathbf{k}}}{\partial \mathbf{k} \partial k_i} A_i \langle c^{\dagger}_{\mathbf{k}\sigma} c_{\mathbf{k}\sigma} \rangle. \qquad 12.$$

As we have seen in the pseudospin picture in Section 2.2, only the diamagnetic coupling contributes to the optical response in the mean-field level with no disorder, resulting in $\mathrm{Re}\,\sigma(\omega) \propto \delta(\omega)$ and $\mathrm{Im}\,\sigma(\omega) \propto 1/\omega$ for the superconducting state. For finite frequency ($\omega \neq 0$), the real part of the optical conductivity vanishes in the BCS clean limit. This does not necessarily mean that the real part of the optical conductivity is suppressed in real experimental situations. For example, in superconductors with a disorder the real part of the optical conductivity is nonzero and not even small for $\omega \neq 0$. In fact, a superconductor NbN used in the experiment of the THG turns out to be close to the dirty regime ($\gamma \gg 2\Delta$, where γ is the impurity scattering rate) as confirmed from the measurement of the optical conductivity (45).

In much the same way as the optical conductivity, the nonlinear response intensity is strongly affected by the impurity effect. The γ dependence of the relative order of magnitudes of the third-order current is summarized in **Table 1**, where $\epsilon_{\rm F}$ is the Fermi energy and the unit of $\mathbf{j}^{(3)}$ is taken such that the diamagnetic-coupling contribution of the quasiparticles is set to be of order 1 (which does not significantly depend on γ). In the BCS clean limit ($\gamma \to 0$), we have only the diamagnetic coupling, for which the Higgs-mode contribution is subleading in the order of $(\Delta/\epsilon_{\rm F})^2$ compared with the quasiparticles. However, in the presence of impurities ($\gamma \neq 0$), the paramagnetic coupling generally emerges to contribute to the THG. Its relative order of magnitude changes as $(\epsilon_{\rm F}\gamma/\Delta^2)^2 \to (\epsilon_{\rm F}/\gamma)^2$ from the clean to dirty limit. The maximum strength of the paramagnetic coupling is achieved around $\gamma \sim \Delta$, where the relative order reaches $(\epsilon_{\rm F}/\Delta)^2$ for both the Higgs mode and quasiparticles. Thus, the impurity scattering drastically enhances the light–Higgs coupling: In the clean limit the Higgs-mode contribution is subleading to quasiparticles, whereas in the dirty regime it becomes comparable with or even larger than the quasiparticle contribution. The precise ratio between the Higgs and quasiparticle contributions may depend on details of the system. Recent studies (52–54) suggest that in the dirty regime the Higgs-mode contribution to THG is an order of magnitude greater than the quasiparticle contribution. An enhancement of the paramagnetic coupling also occurs for strongly coupled superconductors due to the phonon retardation effect (48).

Table 1 Relative order of magnitudes of the third-order current $\mathbf{j}^{(3)}$ in general situations (53)

Mode	Channel	Clean → Dirty
Higgs	Dia ($\mathbf{A}^2$)	$(\Delta/\epsilon_{\rm F})^2$
	Para ($\mathbf{p}\cdot\mathbf{A}$)	$(\epsilon_{\rm F}\gamma/\Delta^2)^2 \to (\epsilon_{\rm F}/\gamma)^2$
Quasiparticles	Dia ($\mathbf{A}^2$)	1
	Para ($\mathbf{p}\cdot\mathbf{A}$)	$(\epsilon_{\rm F}\gamma/\Delta^2)^2 \to (\epsilon_{\rm F}/\gamma)^2$

2.4. Further Developments

So far, we have reviewed the phenomenological and mean-field treatments of the nonlinear light–Higgs coupling for conventional *s*-wave superconductors with or without disorder. For strongly coupled superconductors with an electron–phonon coupling constant $\lambda \gtrsim 1$ [which is the case for NbN superconductors (74–76)], one must take account of strong correlation effects. One useful approach for this is the nonequilibrium dynamical mean-field theory (77), which accounts for local dynamical correlations by mapping a lattice model into a local impurity model embedded in an effective mean field. With this, the Higgs mode has been analyzed in strongly coupled superconductors modeled by the Holstein model (42, 48, 78, 79). A closely related nonequilibrium Keldysh method has been employed to study the Higgs mode in time-resolved photoemission spectroscopy (43, 80) and time-resolved optical conductivity (81). Another approach is to use the gauge-invariant kinetic equation (82–85), in which the shift of the center-of-mass momentum of Cooper pairs (drive effect) caused by a laser pulse has been emphasized.

For multiband superconductors with multiple gaps such as MgB_2, there are not only Higgs modes corresponding to amplitude oscillations of multiple order parameters but also the so-called Leggett mode (86), which corresponds to a collective oscillation of the relative phase between different order parameters. Based on the mean-field theory, possible laser excitations of the Higgs and Leggett modes in multiband superconductors have been studied (53, 87–90).

For non-*s*-wave superconductors, one can expect even richer dynamics of the order parameters. For example, *d*-wave superconductors allow for various symmetries of amplitude modes (91). The quench dynamics of the *d*-wave (92) and $p + ip$-wave (93) Higgs modes have been explored. For recent experimental progresses on pump-probe spectroscopies and THG in *d*-wave superconductors, we refer to Section 3.3. It has also been proposed (94) that by measuring Higgs modes for various quench symmetries one can obtain information on the symmetry of the gap function (Higgs spectroscopy).

3. EXPERIMENTS

In this section, we overview recent progress on experimental observations of the Higgs mode in superconductors. Those include Raman experiments in CDW-coexisting superconductors 2H-$NbSe_2$ and TaS_2 (Section 3.1), THz spectroscopies and THG in a pure *s*-wave superconductor NbN (Section 3.2) and in high-T_c cuprates (Section 3.3), and THz transmittance experiments in NbN under supercurrent injection (Section 3.4).

3.1. Higgs Mode in a Superconductor with Charge-Density Wave

The pioneering work on the observation of the Higgs mode in superconductors dates to 1980 when a Raman experiment was performed in 2H-$NbSe_2$, a transition metal dichalcogenide in which superconductivity coexists with CDW (25, 26). A new peak was observed below T_c that was distinct from the amplitude mode associated with the CDW order. Although it was initially recognized as a pair breaking peak, soon after it was identified as the collective amplitude mode of the superconducting order (i.e., the Higgs mode) (18, 19; see also 27, 63).

A renewed Raman experiment has been conducted recently, revealing the transfer of the oscillator strength from the amplitude mode of CDW (amplitudon) to the Higgs mode (28). Subsequently the Raman experiment under hydrostatic pressure has been performed in 2H-$NbSe_2$ (30) (**Figure 5**). With application of the hydrostatic pressure, the CDW order is suppressed and concomitantly the Raman peak identified as the Higgs mode disappeared, leaving only the Cooper

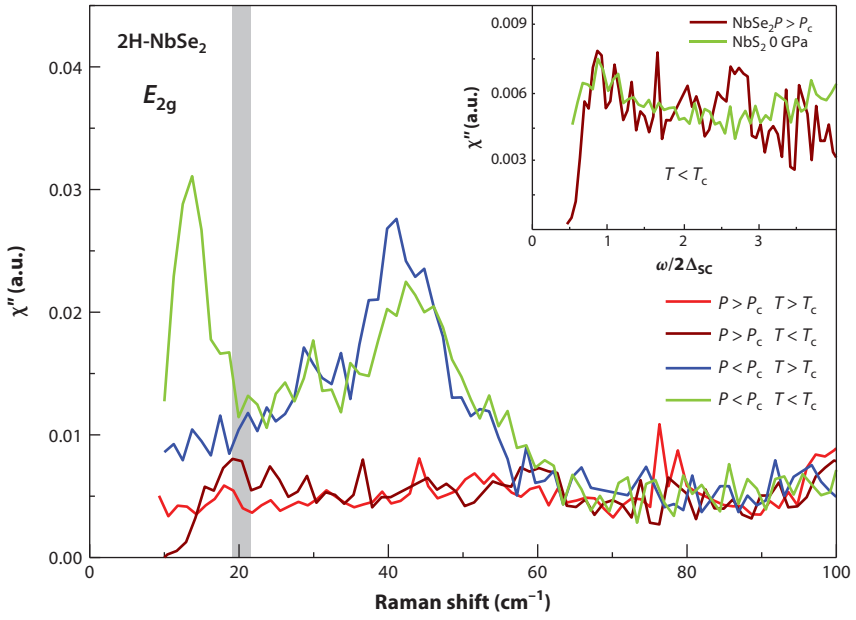

Figure 5

Raman spectra in E_{2g} symmetry of 2H-$NbSe_2$ measured at various temperatures and pressures. Under the ambient pressure ($P < P_c$) and in the superconducting phase ($T < T_c$) (*green*), a sharp peak identified as the Higgs mode appears below the superconducting gap $2\Delta \sim 20$ cm^{-1} marked by the gray vertical line. In the CDW phase ($T > T_c$) (*blue*), only the CDW amplitude mode is observed around 40 cm^{-1}. Under the pressure ($P > P_c$) where CDW collapses, only a pair breaking peak is discerned at $T < T_c$ (*brown*), and no peak is identified at $T > T_c$ (*red*). (*Inset*) Raman spectra in the superconducting state without CDW in 2H-$NbSe_2$ (above 4 GPa) and non-CDW-coexisting NbS_2 (0 GPa), both of which show only the pair breaking peak. Frequency is normalized by 2Δ. Abbreviation: CDW, charge-density wave. Panels adapted from Reference 30 with permission.

pair breaking peak. A clearer separation between the in-gap Higgs mode and the pair breaking peak was recently reported in a similar CDW-coexisting superconductor, TaS_2 (95). These results indicate that the existence of CDW plays an important role on the observability of the Higgs mode in the Raman spectrum. A theoretical study has demonstrated that, due to the coupling of the superconducting order to the coexisting CDW order, the Higgs-mode energy is pushed down below the superconducting gap 2Δ (29). Accordingly, the Higgs mode becomes stable due to the disappearance of the decay channel into the quasiparticle continuum.

3.2. Higgs Mode in a Pure *s*-Wave Superconductor

In "pure" superconductors, where the long-range order such as CDW order does not exist, the observability of the Higgs mode has long been elusive. Here, we show two types of pump-probe experiments: (*a*) nonadiabatic quench, and (*b*) multicycle driving that demonstrates the Higgs mode oscillation in an *s*-wave superconductor NbN. These experiments reveal the observability of the Higgs mode originated from the nonlinear light–Higgs coupling as described in Section 2.

3.2.1. Nonadiabatic quench with a single-cycle terahertz pump pulse. One way to excite the Higgs mode is a nonadiabatic quench of the superconducting state, which can be induced

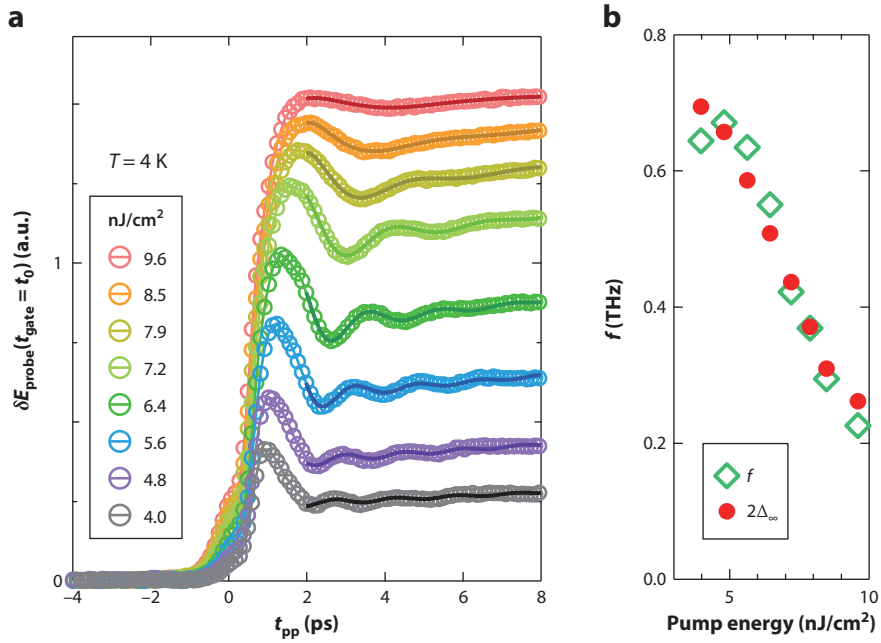

Figure 6

Higgs-mode oscillation after the nonadiabatic excitation of quasiparticles in NbN induced by a monocycle THz pump. (*a*) The temporal evolution of the change of the probe electric field, $\delta E_{\mathrm{probe}}$, as a function of the pump-probe delay time t_{pp} at various pump intensities. The solid curves represent the results fitted by a damped oscillation with a power-law decay. (*b*) The oscillation frequency f obtained from the fits and the asymptotic gap energy $2\Delta_\infty$ as a function of the pump intensity. Panels adapted from Reference 45.

by, for example, a sudden change of the pairing interaction that generates the order-parameter dynamics,

$$\frac{|\Delta(t)|}{\Delta_\infty} \simeq 1 + a\frac{\cos(2\Delta_\infty t + \phi)}{\sqrt{\Delta_\infty t}}, \qquad 13.$$

at long time. Here, $2\Delta_\infty$ is the long-time asymptotic superconducting gap, a is some constant, and ϕ is a phase shift. The behavior (Equation 13) has been theoretically derived on the basis of the time-dependent BCS mean-field theory (16, 33–35). Similar dynamics has also been investigated after a laser-pulse excitation (38–41, 43, 44).

Despite intensive theoretical studies on the Higgs mode in superconductors, the observation of the Higgs mode has long been elusive except for the case of 2H-$NbSe_2$, until the ultrafast THz-pump and THz-probe spectroscopy was performed in a conventional *s*-wave superconductor $Nb_{1-x}Ti_xN$ (45). In this experiment, quasiparticles are instantaneously injected at the superconducting-gap edge to quench the superconducting order parameter nonadiabatically. A strong single-cycle THz-pump pulse with the center frequency around 1 THz (~4 meV) was generated from a $LiNbO_3$ crystal by using the tilted-pulse-front method (96–98), in order to excite high-density quasiparticles just above the gap of $Nb_{1-x}Ti_xN$ thin films with $2\Delta =$ 0.72–1.3 THz (~3.0–5.4 meV) at 4 K. The details of the THz pump–THz probe scheme were given in Reference 99. The subsequent dynamics of the superconducting order parameter was probed by a weaker probe THz pulse in transmission geometry. **Figure 6** shows pump-probe delay dependence of the transmitted probe THz electric field at a fixed point of the probe pulse

waveform, which reflects the order parameter dynamics. A clear oscillation is identified after the pump with the oscillation frequency given by the asymptotic value of the superconducting gap $2\Delta_\infty$ caused by the quasiparticle injection. The decay of the oscillation is well fitted by a power-law decay predicted for the Higgs-mode oscillation. With an increase in the pump intensity, the oscillation period shows a softening, as the asymptotic value of $2\Delta_\infty$ becomes smaller with higher quasiparticle densities. By recording the probe THz waveform at each pump-probe delay, one can extract the dynamics of the complex optical conductivity $\sigma(\omega) = \sigma_1(\omega) + i\sigma_2(\omega)$ (not shown). The spectral-weight oscillation with frequency $2\Delta_\infty$ was clearly identified in both the real and imaginary parts (100), the latter of which reflects the oscillation of the superfluid density.

The intense single-cycle THz pump pulse was crucial to excite the quasiparticles instantaneously at the gap edge, which acts as a nonadiabatic quench of the order parameter, thereby inducing a free oscillation of the Higgs mode. On the contrary, when an IR optical pulse was used as a pump, a relatively slow rise time (~20 ps) was observed for the suppression of the order parameter, though this was dependent on the excitation fluence (99, 101). In this case, the photoexcited hot electrons (holes) emit a large amount of high-frequency phonons (HFPs; $\omega > 2\Delta$), which subsequently induce the Cooper pair–breaking until quasiparticles and HFP reach the quasiequilibrium. This process was well described by the Rothwarf–Taylor phonon-bottleneck model (101); it usually takes a time longer than $(2\Delta)^{-1}$, which breaks the nonadiabatic excitation condition needed for the quench experiment. It should be noted here that even if one uses the near-IR or visible optical excitation, the instantaneous quasiparticle excitation can occur if the stimulated Raman process is efficient (102).

The decay of the Higgs mode is also an important issue. Because the Higgs-mode energy 2Δ coincides with the onset of quasiparticle continuum, the Higgs mode inevitably decays into the quasiparticle continuum even without any collisions (16, 17). However, this does not mean that the Higgs mode is an overdamped mode. In fact, the decay due to the collisionless energy transfer is expected to be proportional to $t^{-1/2}$ in the BCS superconductor, ensuring a much longer lifetime compared with that of the oscillation period. The energy dispersion of the Higgs mode for finite wavenumber q has been calculated as

$$\omega_H \simeq 2\Delta + \frac{v_F^2}{12\Delta}q^2 - i\frac{\pi^2 v_F}{24}q, \qquad 14.$$

where v_F is the Fermi velocity (19). From Equation 14, one can estimate that as the wavenumber q increases and the mode energy enters the quasiparticle continuum, the lifetime of the Higgs mode is shortened and turns into an overdamped mode. For the case of NbN, $\Delta \sim 0.6$ THz and $v_F \sim 2 \times 10^6$ m/s (76), and the imaginary part exceeds the real part in Equation 14 at $q > \Delta/v_F \sim 0.3\ (\mu m)^{-1}$. In the single-cycle THz-pump experiment in a thin film of NbN (45), the value of in-plane wavenumber q estimated from the spot size of the pump (~1 mm) is at most ~1 $(mm)^{-1}$, which is far smaller than Δ/v_F. In such a small q limit, the Higgs mode is considered a well-defined collective mode (19).

3.2.2. Multicycle terahertz driving with subgap frequency and third harmonic generation. To excite the Higgs mode in an on-resonance condition, one can use a narrowband multicycle THz-pump pulse with the photon energy tuned below the superconducting gap 2Δ. With this, the amplitude of the superconducting order parameter was shown to oscillate with twice the frequency of the incident pump-pulse frequency ω during the pulse irradiation (**Figure 7*a–d***) (46). The observed 2ω modulation of the order parameter was attributed to the forced oscillation of the Higgs mode caused by electromagnetic fields. In fact, the time-dependent GL theory shows that there is a coupling term between the Higgs mode (H) and field ($\mathbf{A}$) as expressed by $\mathbf{A}^2 H$

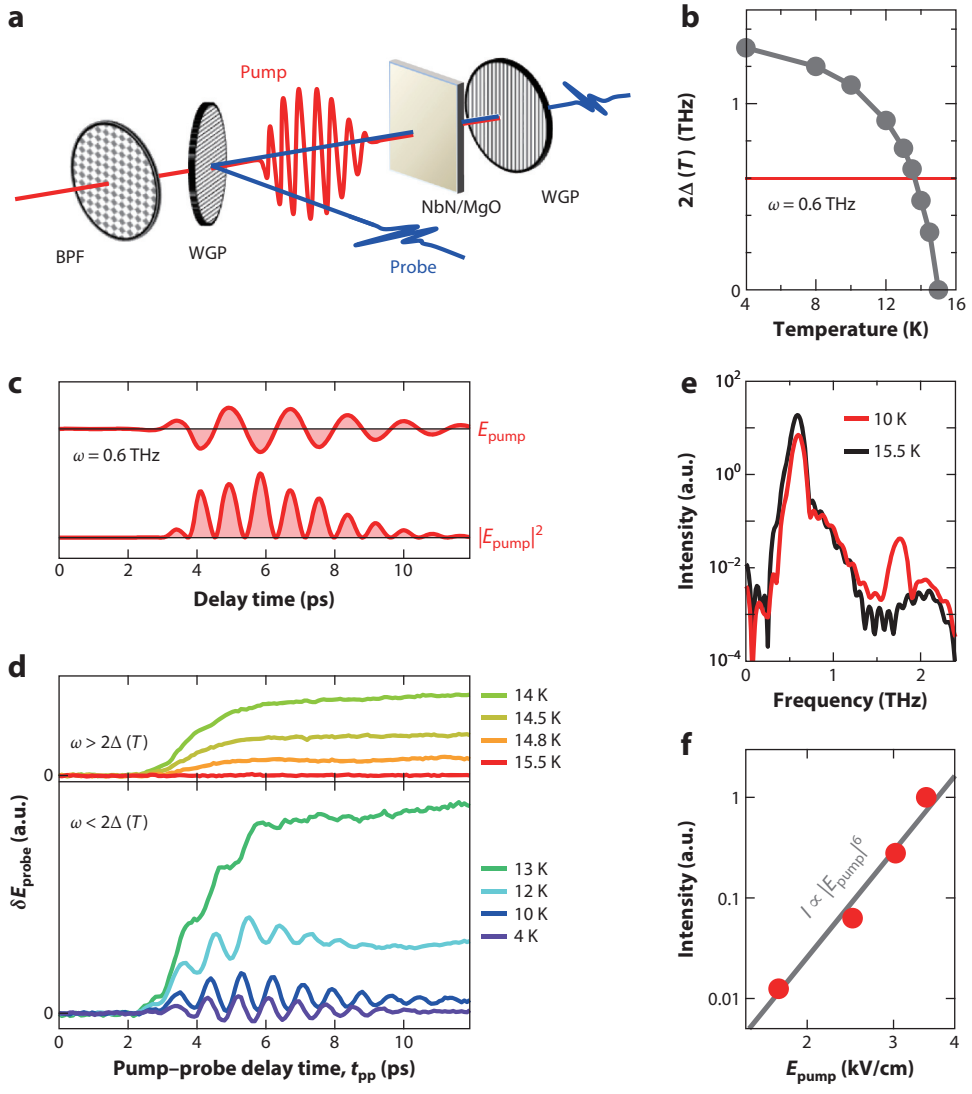

Figure 7

Forced Higgs oscillation and third harmonic generation from a superconducting NbN film under the multicycle THz pump. (*a*) Schematic setup for the multicycle THz pump and THz probe spectroscopy. (*b*) Temperature dependence of the superconducting gap energy. Horizontal line indicates the center frequency of the pump pulse, $\omega = 0.6$ THz. (*c*) Waveform of the pump THz electric field E_{pump} and the squared one, $|E_{\mathrm{pump}}|^2$. (*d*) The change in the transmitted probe THz electric field $\delta E_{\mathrm{probe}}$ as a function of the pump-probe delay time t_{pp} at the temperature range $\omega > 2\Delta(T)$ (*upper*) and $\omega < 2\Delta(T)$ (*lower*). Increase of $\delta E_{\mathrm{probe}}$ corresponds to the reduction of the order parameter. (*e*) Power spectra of the transmitted pump THz pulse above and below $T_{\mathrm{c}} = 15$ K. (*f*) Third harmonic generation intensity as a function of the pump THz field strength. Abbreviations: BPF, bandpass filter; WGP, wire grid polarizer. Panels adapted from Reference 46 with permission.

(Section 2.1), which results in the 2ω-order parameter modulation. The nonlinear electromagnetic response of superconductors has been studied in the frequency range far below 2Δ and near T_c, where the GL theory is applicable (64, 70, 103–105). In the theory developed by Gor'kov & Eliashberg (GE; 70), a closed set of equations for the order parameter Δ and the field $\mathbf{A}$ was derived, which predicts the 2ω modulation of Δ and the THG from the induced supercurrent $\mathbf{j} \propto \mathbf{A}^2\Delta$. The GE theory was experimentally demonstrated through the observation of THG of a microwave field in a paramagnetically doped superconductor (104).

The THz-pump experiments have shed new light on the investigation of the nonlinear electromagnetic response of superconductors at the gap frequency region. After the observation of the 2ω modulation of the order parameter, namely the forced oscillation of the Higgs mode, the THG was observed under the irradiation of a subgap multicycle THz-pump pulse in NbN thin films as shown in **Figure 7*e*,*f***. Importantly, the THG was shown to be resonantly enhanced when the condition $2\omega = 2\Delta$ is satisfied (46). The temperature dependence of THG intensity for various frequencies in an NbN film is shown in **Figure 8**: the temperature dependence of the gap 2Δ and the incident frequencies (**Figure 8*a***); the raw data of THG intensities (**Figure 8*b***), those normalized by the internal field inside the superconducting film that is proportional to the third-order susceptibility $|\chi^{(3)}|^2$ (**Figure 8*c***); and the THG intensity further normalized by the proportional factor of the THG intensity $\Delta(T)^4$ versus the frequency normalized to the gap, $2\omega/2\Delta(T)$ (**Figure 8*d***). These results clearly show the two-photon resonances of the Higgs mode with the field.

As previously described in Section 2.3, however, it was theoretically pointed out that there is a contribution also from the quasiparticle excitation (i.e., CDFs) in THG, which also exhibits the $2\omega = 2\Delta$ resonance (47). Within the BCS mean-field approximation in the clean limit, the quasiparticle term was shown to exceed the Higgs mode contribution in THG. At the same time, it was predicted that the THG from the quasiparticle term should exhibit polarization dependence with respect to the crystal axis while the Higgs term is totally isotropic in a square lattice (47). In the experiments in NbN, the THG intensity was shown to be independent from the incident polarization angle with respect to the crystal orientation, and notably the emitted THG does not have orthogonal components with respect to the incident polarization of the fundamental (ω) wave (49). Such a totally isotropic nature of THG cannot be well accounted for by the CDF term even if one considers the crystal symmetry of NbN (50) and indicates the Higgs mode as the origin of THG. Recently, the importance of $\mathbf{p} \cdot \mathbf{A}$ term on the coupling between the Higgs mode and the gauge field was elucidated. In particular, the $\mathbf{p} \cdot \mathbf{A}$ term contribution is largely enhanced when one considers the phonon retardation effect beyond the BCS approximation (48) and more prominently when one considers the nonmagnetic impurity scattering effect (52–54), dominating the quasiparticle term by an order of magnitude as described in Section 2.3. This paramagnetic term was also shown to dominate the diamagnetic term, although its ratio depends on the ratio between the coherence length and the mean free path. The NbN superconductor is in the dirty regime as manifested by a clear superconducting gap structure observed in the optical conductivity spectrum, and the paramagnetic term should significantly contribute to THG.

3.3. Higgs Mode in High-T_c Cuprates

Higgs modes can exist not only in *s*-wave superconductors but also in unconventional superconductors. For example, in *d*-wave superconductors such as high-T_c cuprates one can expect various types of collective modes, including not only the totally isotropic oscillation of the gap function in relative momentum space (A_{1g} mode) but also those that oscillate anisotropically (e.g., A_{2g}, B_{1g}, and B_{2g} modes) (91). These are reminiscent of Bardasis–Schrieffer mode for the case of *s*-wave

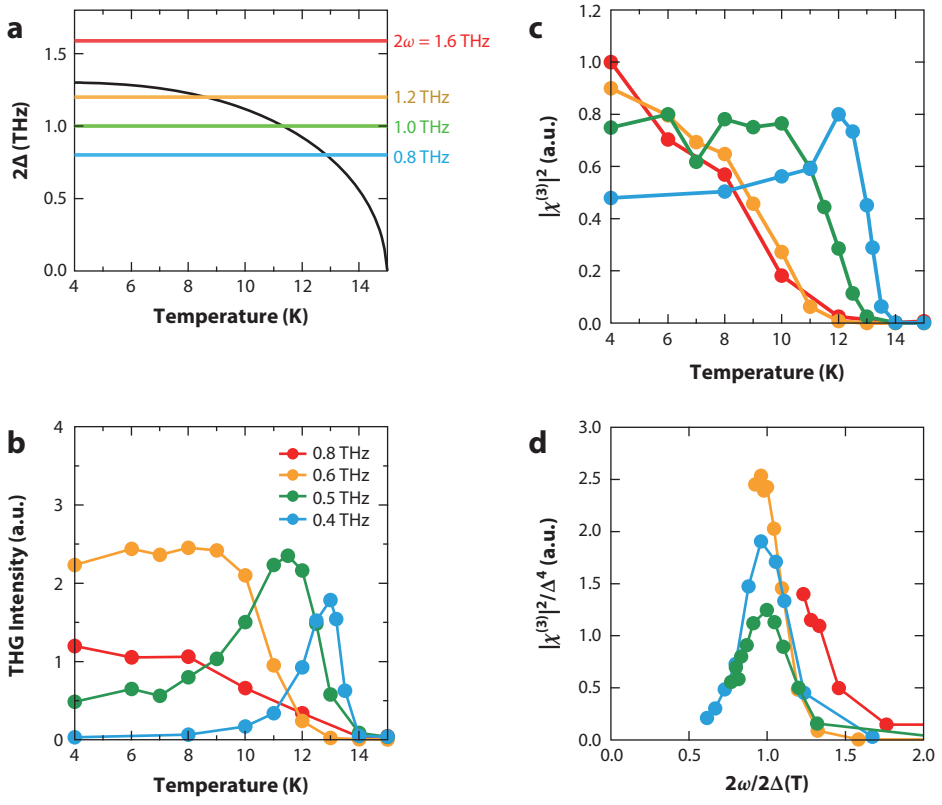

Figure 8

Temperature dependence of THG signal from NbN. (*a*) Temperature dependence of the superconducting gap $2\Delta(T)$. Two times the THz pump frequency, 2ω, is shown by a horizontal line. (*b*) Measured THG intensities at each frequency as a function of temperature. (*c*) THG intensities normalized by the temperature-dependent internal field inside the superconducting film and the transmittance of the THG signal, which corresponds to the susceptibility of THG, $|\chi^{(3)}|^2$. (*d*) Further normalized value of $|\chi^{(3)}|^2$ by the temperature-dependent gap $\Delta(T)^4$ as a function of normalized frequency $2\omega/2\Delta(T)$. Relative intensities between different frequencies are arbitrary. Abbreviation: THG, third harmonic generation. Data taken from Reference 100.

superconductors (106). Possible collective modes have been classified based on the point group symmetry of the lattice (91), and the relaxation behavior of the A_{1g} mode induced by a quench has been discussed (92). A theoretical proposal has been made to observe the Higgs mode in a *d*-wave superconductor through time- and angle-resolved photoemission spectroscopy (80).

The observation of the Higgs mode in *d*-wave superconductors was recently made in THz-pump and optical-probe experiments in high-T_c cuprates, $Bi_2Sr_2CaCu_2O_{8+x}$ (Bi2212) (55). An oscillatory signal of the optical reflectivity that follows the squared THz electric field was observed, which is markedly enhanced below T_c, as shown in **Figure 9**. This signal was interpreted as the THz-pump-induced optical Kerr effect, namely the third-order nonlinear effect induced by the intense THz-pump pulse. In the Bi2212 system, both A_{1g} and B_{1g} symmetry components with respect to the polarization-angle dependence (which should be distinguished from the relative-momentum symmetry classification mentioned above) were observed in the THz-Kerr signal. The doping dependence shows that the A_{1g} component is dominant in all the measured samples from the under to the near-optimal region. From the comparison with the BCS

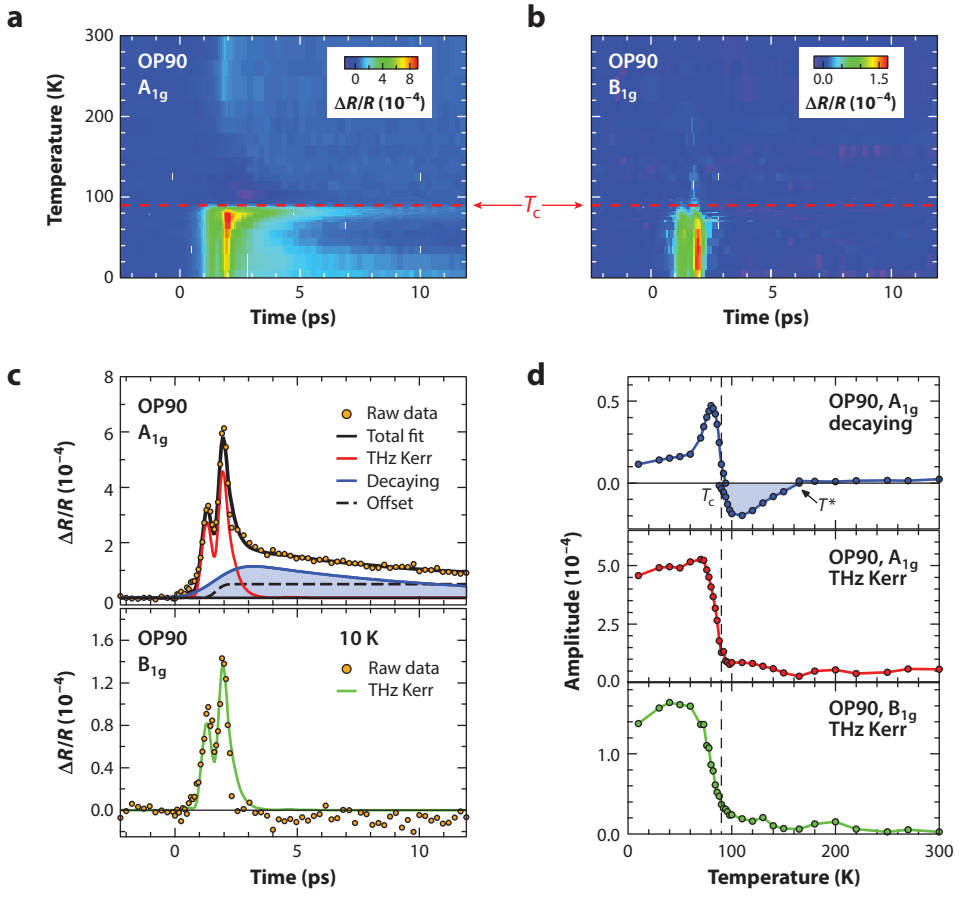

Figure 9

Forced oscillation of Higgs mode in an optimally doped (OP90) $Bi_2Sr_2CaCu_2O_{8+x}$ measured by THz pump and optical reflection probe experiment. Temperature dependencies of reflectivity change $\Delta R/R$ as a function of pump-probe delay time in (*a*) A_{1g} and (*b*) B_{1g} components. Red dashed lines indicate T_c. (*c*) The A_{1g} and B_{1g} components against the pump-probe delay time at 10 K. Fitting curves are also shown by solid lines. (*d*) Temperature dependencies of the A_{1g} decaying component (*blue*, incoherent quasiparticle excitation), the A_{1g} oscillatory component (*red*, forced Higgs oscillation), and the B_{1g} oscillatory component (*green*, likely the charge-density fluctuation). Figure adapted from Reference 55.

calculation of the nonlinear susceptibility, the A_{1g} component was assigned to be the *d*-wave Higgs-mode contribution.

The observed oscillatory signal corresponds to the 2ω modulation of the order parameter as observed in an *s*-wave NbN superconductor under the subgap multicycle THz-pump irradiation. Accordingly, like in the case of *s*-wave systems, one can expect the THG signal from high-T_c cuprates. Recently, THG was indeed observed ubiquitously in $La_{1.84}Sr_{0.16}CuO_4$, $DyBa_2Cu_3O_{7-x}$, $YBa_2Cu_3O_{7-x}$, and overdoped $Bi_2Sr_2CaCu_2O_{8+x}$ (56) by using a 0.7-THz coherent and intense light source at the TELBE [high-field high-repetition-rate Terahertz facility at ELBE (Electron Linac for beams with high Brilliance and low Emittance)] beamline at Helmholtz Zentrum Dresden Rossendorf.

3.4. Higgs Mode in the Presence of Supercurrents

So far, we have seen the Higgs mode excitation by the nonadiabatic quench with instantaneous quasiparticle injection or through the quadratic coupling with the electromagnetic wave. Recently, it has been theoretically shown that when there is a condensate flow (i.e., supercurrent), the Higgs mode linearly interacts with electromagnetic waves with the electric field polarized along the direction of the supercurrent flow (57). Namely, the Higgs mode should be observed in the optical conductivity spectrum at the superconducting gap $\omega = 2\Delta$ under the supercurrent injection. This effect is explained by the momentum term in the action, $S \propto \int \mathbf{Q}^2(t)|\Delta(t)|^2 \mathrm{d}t\mathrm{d}r$, where $\mathbf{Q}(t) = \mathbf{Q}_0 + \mathbf{Q}_\Omega(t)$ is the gauge-invariant momentum of the condensate, $\mathbf{Q}_0$ is the dc supercurrent part, and $\mathbf{Q}_\Omega(t) = \mathrm{Re}[\mathbf{Q}_\Omega \exp(i\Omega t)]$ is the time-dependent part driven by the ac probe field, respectively. $\Delta(t) = \Delta_0 + \delta\Delta(t)$ is the time-dependent superconducting order parameter. The action S includes the integral of $\delta\Delta_{2\Omega}\mathbf{Q}^2_{-\Omega}$ and $\delta\Delta_\Omega\mathbf{Q}_0\mathbf{Q}_{-\Omega}$, where $\delta\Delta_{\Omega(2\Omega)}$ is the Fourier component of the oscillating order parameter. The first term corresponds to the quadratic coupling of the Higgs mode to the gauge field as described in Section 2. The second term indicates that the Higgs mode linearly couples with the gauge field under the supercurrent with the condensate momentum $\mathbf{Q}_0$ parallel to the probe electric field.

Recently, in accordance with the theoretical prediction, the Higgs mode was observed in the optical conductivity in an *s*-wave superconductor NbN thin film under the supercurrent injection by using THz time-domain spectroscopy (58). **Figure 10*a*** shows the schematic experimental

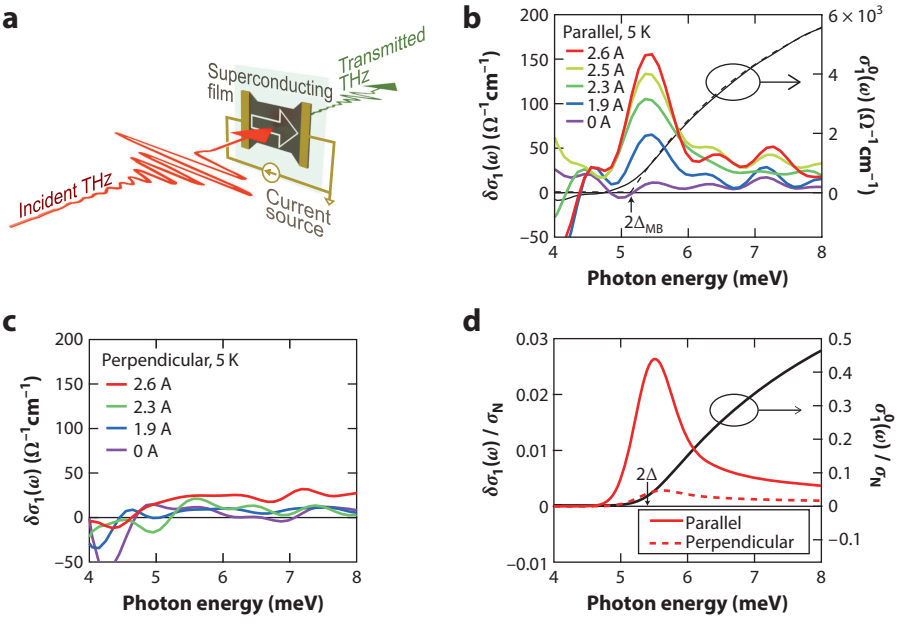

Figure 10

(*a*) Schematic view of the THz transmittance experiments under supercurrent injection. The change of the optical conductivity induced by supercurrent injection taken with the THz probe electric field (*b*) parallel or (*c*) perpendicular to the current direction. The optical conductivity spectra measured without the current is also plotted in panel *b*. The dashed line represents a fit by the Mattis–Bardeen model (107, 108), and the superconducting gap estimated from the fit is indicated by the vertical arrow. (*d*) Theoretically expected changes of optical conductivity induced by the supercurrent injection with respect to the normal state conductivity σ_N. Panels adapted from Reference 58.

setup. **Figure 10*b*,*c*** shows the change of the real part of the optical conductivity induced by the supercurrent injection with the probe polarization (**Figure 10*b***) parallel and (**Figure 10*c***) orthogonal to the current direction. A clear peak is observed at the gap edge $\omega = 2\Delta$ in the parallel geometry, showing good agreement with the spectra calculated on the basis of the theory developed by Moor et al. (57) as represented in **Figure 10*d***. This result indicates that, without resorting to the sophisticated nonlinear THz spectroscopy, the Higgs mode can be observed in the linear response function when the condensate has a finite momentum, expanding the feasibility for the detection of the Higgs mode in a wider range of materials.

The visibility of the Higgs mode in the optical conductivity has also been addressed in a two-dimensional system near a quantum critical point (109, 110; see also 111 and 112). Experimentally, an extra spectral weight in the optical conductivity below the superconducting gap was observed in a strongly disordered superconducting film of NbN, which was interpreted in terms of the Higgs mode with its mass pushed below the pair breaking gap due to the strong disorder (113). However, the assignment of the extra spectral weight below the gap remains under debate. It can also be described by the NG mode, which acquires the electric dipole in strongly disordered superconductors (114–117). The extra optical conductivity was also accounted for by the disorder-induced broadening of the quasiparticle density of states below the gap (118).

4. FUTURE PERSPECTIVE

Having seen the Higgs mode in *s*-wave and *d*-wave superconductors, it is fascinating to extend the observation of the Higgs mode to a variety of conventional/unconventional superconductors. The study of the Higgs mode in multiband superconductors would be important, as it would give deeper insights into the interband couplings. For instance, the application of the nonlinear THz spectroscopy to iron-based superconductors is highly intriguing, as it may provide information on the interband interactions and pairing symmetry (87, 119, 120). The Leggett mode, namely the collective mode associated with the relative phase of two condensates (86), is also expected to be present in multiband superconductors. The Leggett mode has been observed in a multiband superconductor MgB_2 by Raman spectroscopy (121). The nonlinear coupling between the Leggett mode and THz light has also been discussed (53, 87–90). Recently, a THz-pump-THz-probe study in MgB_2 has been reported, and the results were interpreted in terms of the Leggett mode (122). However, the dominant contribution of the Higgs mode over the Leggett mode in the nonlinear THz responses was theoretically pointed out in the case of dirty-limit superconductors (53). Therefore, further experimental verification of the Higgs and Leggett modes is left as a future problem.

The fate of the behavior of the Higgs mode in a strongly correlated regime and, what is more, in a BCS-BEC (Bose–Einstein condensate) crossover regime is an intriguing problem. In particular, the decay profile of the Higgs mode has been predicted to change from the BCS to BEC regime (36, 37, 123–125). Experimentally, such a study has been realized in a cold-atom system, showing a broadening of the Higgs mode in the BEC regime (61). Further investigation on the Higgs mode in the BCS-BEC crossover regime will be a future challenge in solid-state systems.

The Higgs mode in spin-triplet *p*-wave superconductors is another issue to be explored in the future. Like in the case of superfluid ^{3}He (22, 59, 126), multiple Higgs modes are expected to appear due to the spontaneous symmetry breaking in the spin channel, and its comparison with high-energy physics would be interesting.

In another new paradigm, the observation of the Higgs mode would pave a new pathway for the study of nonequilibrium phenomena, particularly for the photoinduced superconductivity (127–130). Being a fingerprint of the order parameter with a picosecond time resolution,

the observation of the Higgs mode in photoinduced states should offer direct evidence for nonequilibrium superconductivity. In strongly correlated electron systems exemplified by the unconventional superconductors, elucidation of the interplay between competing and/or coexisting orders with superconductivity is an important issue for understanding the emergent phases. The time-domain study of collective modes associated with those orders is expected to provide new insights for their interplay.

DISCLOSURE STATEMENT

The authors are not aware of any affiliations, memberships, funding, or financial holdings that might be perceived as affecting the objectivity of this review.

ACKNOWLEDGMENTS

We acknowledge valuable discussions with Hideo Aoki, Yann Gallais, Dirk Manske, Stefan Kaiser, and Seiji Miyashita. We also acknowledge coworkers Yuta Murotani, Keisuke Tomita, Kota Katsumi, Sachiko Nakamura, Naotaka Yoshikawa, and in particular Ryusuke Matsunaga for fruitful discussions and their support for preparing the manuscript.

LITERATURE CITED

1. Nambu Y. 2011. *BCS: 50 Years*, ed. LN Cooper, D Feldman. Singapore: World Sci.
2. Ginzburg VL, Landau LD. 1950. *Zh. Eksp. Teor. Fiz.* 20:1064–82
3. Bogoliubov NN. 1958. *J. Exp. Theoret. Phys.* 34:58–65
4. Anderson PW. 1958. *Phys. Rev.* 110:827–35
5. Anderson PW. 1958. *Phys. Rev.* 112:1900–16
6. Nambu Y. 1960. *Phys. Rev.* 117:648–63
7. Goldstone J. 1961. *Nuovo Cim.* 19:154–64
8. Goldstone J, Salam A, Weinberg S. 1962. *Phys. Rev.* 127:965–70
9. Anderson PW. 1963. *Phys. Rev.* 130:439–42
10. Englert F, Brout R. 1964. *Phys. Rev. Lett.* 13:321–23
11. Higgs PW. 1964. *Phys. Lett.* 12:132–33
12. Higgs PW. 1964. *Phys. Rev. Lett.* 13:508–9
13. Guralnik GS, Hagen CR, Kibble TWB. 1964. *Phys. Rev. Lett.* 13:585–87
14. Anderson PW. 2015. *Nat. Phys.* 11:93
15. Bardeen J, Cooper LN, Schrieffer JR. 1957. *Phys. Rev.* 108:1175–204

15a. Schmid A. 1968. *Phys. Kond. Mater.* 8:129–40

16. Volkov AF, Kogan SM. 1974. *Sov. Phys. J. Exp. Theoret. Phys.* 38:1018–21
17. Kulik IO, Entin-Wohlman O, Orbach R. 1981. *J. Low Temp. Phys.* 43:591–620
18. Littlewood PB, Varma CM. 1981. *Phys. Rev. Lett.* 47:811–14
19. Littlewood PB, Varma CM. 1982. *Phys. Rev. B* 26:4883–93
20. Nambu Y, Jona-Lasinio G. 1961. *Phys. Rev.* 122:345–58
21. Nambu Y. 1985. *Physica* 15D:147–51
22. Volovik GE, Zubkov MA. 2014. *J. Low Temp. Phys.* 175:486–97
23. ATLAS Collab. 2012. *Phys. Lett. B* 716:1–29
24. CMS Collab. 2012. *Phys. Lett. B* 716:30–61
25. Sooryakumar R, Klein MV. 1980. *Phys. Rev. Lett.* 45:660–62
26. Sooryakumar R, Klein MV. 1981. *Phys. Rev. B* 23:3213–21
27. Varma C. 2002. *J. Low Temp. Phys.* 126:901–9
28. Méasson MA, Gallais Y, Cazayous M, Clair B, Rodière P, et al. 2014. *Phys. Rev. B* 89:060503(R)

29. Cea T, Benfatto L. 2014. *Phys. Rev. B* 90:224515
30. Grasset R, Cea T, Gallais Y, Cazayous M, Sacuto A, et al. 2018. *Phys. Rev. B* 97:094502
31. Barankov RA, Levitov LS, Spivak BZ. 2004. *Phys. Rev. Lett.* 93:160401
32. Yuzbashyan EA, Altshuler BL, Kuznetsov VB, Enolskii VZ. 2005. *Phys. Rev. B* 72:220503
33. Barankov RA, Levitov LS. 2006. *Phys. Rev. Lett.* 96:230403
34. Yuzbashyan EA, Tsyplyatyev O, Altshuler BL. 2006. *Phys. Rev. Lett.* 96:097005
35. Yuzbashyan EA, Dzero M. 2006. *Phys. Rev. Lett.* 96:230404
36. Gurarie V. 2009. *Phys. Rev. Lett.* 103:075301
37. Tsuji N, Eckstein M, Werner P. 2013. *Phys. Rev. Lett.* 110:136404
38. Papenkort T, Axt VM, Kuhn T. 2007. *Phys. Rev. B* 76:224522
39. Papenkort T, Kuhn T, Axt VM. 2008. *Phys. Rev. B* 78:132505
40. Schnyder AP, Manske D, Avella A. 2011. *Phys. Rev. B* 84:214513
41. Krull H, Manske D, Uhrig GS, Schnyder AP. 2014. *Phys. Rev. B* 90:014515
42. Tsuji N, Aoki H. 2015. *Phys. Rev. B* 92:064508
43. Kemper AF, Sentef MA, Moritz B, Freericks JK, Devereaux TP. 2015. *Phys. Rev. B* 92:224517
44. Chou Y-Z, Liao Y, Foster MS. 2017. *Phys. Rev. B* 95:104507
45. Matsunaga R, Hamada YI, Makise K, Uzawa Y, Terai H, et al. 2013. *Phys. Rev. Lett.* 111:057002
46. Matsunaga R, Tsuji N, Fujita H, Sugioka A, Makise K, et al. 2014. *Science* 345:1145–49
47. Cea T, Castellani C, Benfatto L. 2016. *Phys. Rev. B* 93:180507(R)
48. Tsuji N, Murakami Y, Aoki H. 2016. *Phys. Rev. B* 94:224519
49. Matsunaga R, Tsuji N, Makise K, Terai H, Aoki H, Shimano R. 2017. *Phys. Rev. B* 96:020505(R)
50. Cea T, Barone P, Castellani C, Benfatto L. 2018. *Phys. Rev. B* 97:094516
51. Jujo T. 2015. *J. Phys. Soc. Jpn.* 84:114711
52. Jujo T. 2018. *J. Phys. Soc. Jpn.* 87:024704
53. Murotani Y, Shimano R. 2019. *Phys. Rev. B* 99:224510
54. Silaev M. 2019. *Phys. Rev. B* 99:224511
55. Katsumi K, Tsuji N, Hamada YI, Matsunaga R, Schneeloch J, et al. 2018. *Phys. Rev. Lett.* 120:117001
56. Chu H, Kim M-J, Katsumi K, Kovalev S, Dawson RD, et al. 2019. arXiv:1901.06675
57. Moor A, Volkov AF, Efetov KB. 2017. *Phys. Rev. Lett.* 118:047001
58. Nakamura S, Iida Y, Murotani Y, Matsunaga R, Terai H, Shimano R. 2019. *Phys. Rev. Lett.* 122:257001
59. Vollhardt D, Wölfle P. 1990. *The Superfluid Phases of Helium 3*. London: Taylor & Francis
60. Endres M, Fukuhara T, Pekker D, Cheneau M, Schauβ P, et al. 2012. *Nature* 487:454–58
61. Behrle A, Harrison T, Kombe J, Gao K, Link M, et al. 2018. *Nat. Phys.* 14:781–85
62. Rüegg C, Normand B, Matsumoto M, Furrer A, McMorrow DF, et al. 2008. *Phys. Rev. Lett.* 100:205701
63. Pekker D, Varma CM. 2015. *Annu. Rev. Condens. Matter Phys.* 6:269–97
64. Abraham E, Tsuneto T. 1966. *Phys. Rev.* 152:416–32
65. Schmid A. 1966. *Phys. Kond. Mater.* 5:302–17
66. Caroli C, Maki K. 1967. *Phys. Rev.* 159:306–15
67. Ebisawa H, Fukuyama H. 1971. *Prog. Theoret. Phys.* 46:1042–53
68. Sá de Melo CAR, Randeria M, Engelbrecht JR. 1993. *Phys. Rev. Lett.* 71:3202–5
69. Tsuchiya S, Yamamoto D, Yoshii R, Nitta M. 2018. *Phys. Rev. B* 98:094503
70. Gor'kov LP, Eliashberg GM. 1968. *Sov. Phys. J. Exp. Theoret. Phys.* 27:328–34
71. Gulian AM, Zharkov GF. 1999. *Nonequilibrium Electrons and Phonons in Superconductors*. New York: Kluwer Acad./Plenum Publ.
72. Kopnin N. 2001. *Theory of Nonequilibrium Superconductivity*. Oxford, UK: Oxford Univ. Press
73. Schrieffer JR. 1999. *Theory of Superconductivity*. Boca Raton: CRC Press
74. Kihlstrom KE, Simon RW, Wolf SA. 1985. *Phys. Rev. B* 32:1843–45(R)
75. Brorson SD, Kazeroonian A, Moodera JS, Face DW, Cheng TK, et al. 1990. *Phys. Rev. Lett.* 64:2172–75
76. Chockalingam SP, Chand M, Jesudasan J, Tripathi V, Raychaudhuri P. 2008. *Phys. Rev. B* 77:214503
77. Aoki H, Tsuji N, Eckstein M, Kollar M, Oka T, Werner P. 2014. *Rev. Mod. Phys.* 86:779–837
78. Murakami Y, Werner P, Tsuji N, Aoki H. 2016. *Phys. Rev. B* 93:094509
79. Murakami Y, Werner P, Tsuji N, Aoki H. 2016. *Phys. Rev. B* 94:115126

80. Nosarzewski B, Moritz B, Freericks JK, Kemper AF, Devereaux TP. 2017. *Phys. Rev. B* 96:184518
81. Kumar A, Kemper AF. 2019. arXiv:1902.09549
82. Yu T, Wu MW. 2017. *Phys. Rev. B* 96:155311
83. Yu T, Wu MW. 2017. *Phys. Rev. B* 96:155312
84. Yang F, Wu MW. 2018. *Phys. Rev. B* 98:094507
85. Yang F, Wu MW. 2019. *Phys. Rev. B* 100:104513
86. Leggett AJ. 1966. *Prog. Theor. Phys.* 36:901–30
87. Akbari A, Schnyder AP, Manske D, Eremin I. 2013. *Europhys. Lett.* 101:17002
88. Krull H, Bittner N, Uhrig GS, Manske D, Schnyder AP. 2016. *Nat. Commun.* 7:11921
89. Cea T, Benfatto L. 2016. *Phys. Rev. B* 94:064512
90. Murotani Y, Tsuji N, Aoki H. 2017. *Phys. Rev. B* 95:104503
91. Barlas Y, Varma CM. 2013. *Phys. Rev. B* 87:054503
92. Peronaci F, Schiró M, Capone M. 2015. *Phys. Rev. Lett.* 115:257001
93. Foster MS, Dzero M, Gurarie V, Yuzbashyan EA. 2013. *Phys. Rev. B* 88:104511
94. Fauseweh B, Schwarz L, Tsuji N, Cheng N, Bittner N, et al. 2017. arXiv:1712.07989
95. Grasset R, Gallais Y, Sacuto A, Cazayous M, Mañas-Valero S, et al. 2019. *Phys. Rev. Lett.* 122:127001
96. Hebling J, Yeh KL, Hoffmann MC, Bartal B, Nelson KA. 2008. *J. Opt. Soc. Am. B* 25:B6–19
97. Watanabe S, Minami N, Shimano R. 2011. *Opt. Express* 19:1528–38
98. Shimano R, Watanabe S, Matsunaga R. 2012. *J. Infrared Millim. Terahertz Waves* 33:861–69
99. Matsunaga R, Shimano R. 2012. *Phys. Rev. Lett.* 109:187002
100. Matsunaga R, Shimano R. 2017. *Phys. Scr.* 92:024003
101. Beck M, Klammer M, Lang S, Leiderer P, Kabanov VV, et al. 2011. *Phys. Rev. Lett.* 107:177007
102. Mansart B, Lorenzana J, Mann A, Odeh A, Scarongella M, et al. 2013. *PNAS* 110:4539–44
103. Gor'kov LP, Eliashberg GM. 1969. *Sov. Phys. J. Exp. Theoret. Phys.* 29:698–703
104. Amato JC, McLean WL. 1976. *Phys. Rev. Lett.* 37:930–33
105. Entin-Wohlman O. 1978. *Phys. Rev. B* 18:4762–67
106. Bardasis A, Schrieffer JR. 1961. *Phys. Rev.* 121:1050–62
107. Mattis DC, Bardeen J. 1958. *Phys. Rev.* 111:412–17
108. Zimmermann W, Brandt EH, Bauer M, Seider E, Genzel L. 1991. *Phys. C: Supercondens.* 183:99–104
109. Podolsky D, Auerbach A, Arovas DP. 2011. *Phys. Rev. B* 84:174522
110. Gazit S, Podolsky D, Auerbach A. 2013. *Phys. Rev. Lett.* 110:140401
111. Sachdev S. 1999. *Phys. Rev. B* 59:14054–73
112. Zwerger W. 2004. *Phys. Rev. Lett.* 92:027203
113. Sherman D, Pracht US, Gorshunov B, Poran S, Jesudasan J, et al. 2015. *Nat. Phys.* 11:188–92
114. Cea T, Bucheli D, Seibold G, Benfatto L, Lorenzana J, Castellani C. 2014. *Phys. Rev. B* 89:174506
115. Cea T, Castellani C, Seibold G, Benfatto L. 2015. *Phys. Rev. Lett.* 115:157002
116. Pracht US, Cea T, Bachar N, Deutscher G, Farber E, et al. 2017. *Phys. Rev. B* 96:094514
117. Seibold G, Benfatto L, Castellani C. 2017. *Phys. Rev. B* 96:144507
118. Cheng B, Wu L, Laurita NJ, Singh H, Chand M, et al. 2016. *Phys. Rev. B* 93:180511
119. Maiti S, Hirschfeld PJ. 2015. *Phys. Rev. B* 92:094506
120. Müller MA, Shen P, Dzero M, Eremin I. 2018. *Phys. Rev. B* 98:024522
121. Blumberg G, Mialitsin A, Dennis BS, Klein MV, Zhigadlo ND, Karpinski J. 2007. *Phys. Rev. Lett.* 99:227002
122. Giorgianni F, Cea T, Vicario C, Hauri CP, Withanage WK, et al. 2019. *Nat. Phys.* 15:341–46
123. Scott RG, Dalfovo F, Pitaevskii LP, Stringari S. 2012. *Phys. Rev. A* 86:053604
124. Yuzbashyan EA, Dzero M, Gurarie V, Foster MS. 2015. *Phys. Rev. A* 91:033628
125. Tokimoto J, Tsuchiya S, Nikuni T. 2019. *J. Phys. Soc. Jpn.* 88:023601
126. Wölfle P. 1977. *Physica B* 90:96–106
127. Fausti D, Tobey RI, Dean N, Kaiser S, Dienst A, et al. 2011. *Science* 331:189–91
128. Kaiser S, Hunt CR, Nicoletti D, Hu W, Gierz I, et al. 2014. *Phys. Rev. B* 89:184516
129. Hu W, Kaiser S, Nicoletti D, Hunt CR, Gierz I, et al. 2014. *Nat. Mater.* 13:705–11
130. Mitrano M, Cantaluppi A, Nicoletti D, Kaiser S, Perucchi A, et al. 2016. *Nature* 530:461–64